scientific reports

Check for updates

OPEN

Antibody profiling and plasma proteomics in SARS-CoV-2 infection: a pilot study

Tetsuya Fukuda[1]✉, Aya Nakayama[2], Yoko Chikaoka[2], Yasuhiko Bando[1] & Takeshi Kawamura[2]✉

We present a pilot, single-subject longitudinal analysis of plasma antibodies and proteome dynamics across 310 days spanning COVID-19 vaccination and subsequent SARS-CoV-2 infection. Serial plasma samples were analyzed by DIA-LC-MS/MS, identifying 1502 proteins. Comparative analyses across key intervals (pre-vaccination, post-dose 1, post-dose 2, and post-infection) showed minimal proteomic shifts after vaccination but distinct, coordinated expression changes after SARS-CoV-2 infection.

Keywords SARS-CoV-2, COVID-19, Plasma proteomics, Data-independent acquisition (DIA), Pilot study

The novel coronavirus SARS-CoV-2, discovered in 2019, causes coronavirus disease 2019 (COVID-19) and rapidly led to a global pandemic, spreading worldwide and causing numerous infections and fatalities. Researchers worldwide have responded swiftly, focusing on the rapid development of treatments and vaccines. The approved medications were also quickly put into practical use and introduced onto the market. However, like other RNA viruses, SARS-CoV-2 has continuously evolved, giving rise to multiple variants over the course of the pandemic. While some reports have suggested that certain later-emerging variants may be associated with reduced clinical severity at the population level, substantial uncertainty remains, and continued vigilance is required[1–4].

Since the early stages of the COVID-19 pandemic, our research group has been monitoring endogenous antibody responses to SARS-CoV-2 in human subjects and has collected and stored a large number of clinical plasma samples. In-depth proteomic analysis can be performed on the obtained plasma samples, particularly those taken before and after COVID-19 vaccination and infection. This can reveal how infection progresses through the variations and behaviors of specific proteins indicative of immune responses, particularly those proteins with fluctuating profiles.

In this study, blood samples were collected from a single research volunteer prior to the administration of the COVID-19 vaccination. Sequential sampling was conducted, covering the first vaccine dose (Moderna), the second dose (Moderna), subsequent SARS-CoV-2 infection, and ongoing periodic sampling thereafter. Antibody testing was carried out on the obtained samples, along with the measurement and evaluation of antibody titers. Additionally, a time series protein profile was obtained through proteomic analysis.

For proteomic analysis via LC-MS, the DIA-LC-MS method was applied[5–8]. DIA-LC-MS differs from conventional LC-MS proteomic analysis, in which only peptide-like spectra are selected from the MS spectrum of single MS in the first stage and then subjected to successive MS/MS. LC-MS proteomic analysis thus has limitations in terms of the number of MS/MS events due to the performance of the mass spectrometer. Weak peaks and similar components may be overlooked as a result. In contrast, with DIA-LC-MS, in DIA mode, for example, by segmenting the MS range, such as m/z 425–445, into segments of m/z 20 each, all the observed peaks in that range are collectively subjected to MS/MS. As a result, the identification count tends to increase compared with that of conventional shotgun LC-MS proteomic analysis.

In addition to antibody testing, we conducted DIA-LC-MS-based proteome analysis on the same plasma samples (Fig. 1). Through this process, a quantitative protein profile was obtained, and the behavior of proteins expressed within the sampled time series was verified. In this report, we provide an account of our findings.

[1]Research and Developments, Biosys Technologies, Inc., Tokyo, Japan. [2]Isotope Science Center, The University of Tokyo, Tokyo, Japan. ✉email: t-fukuda@biosys-tech.co.jp; kawamura@lsbm.org

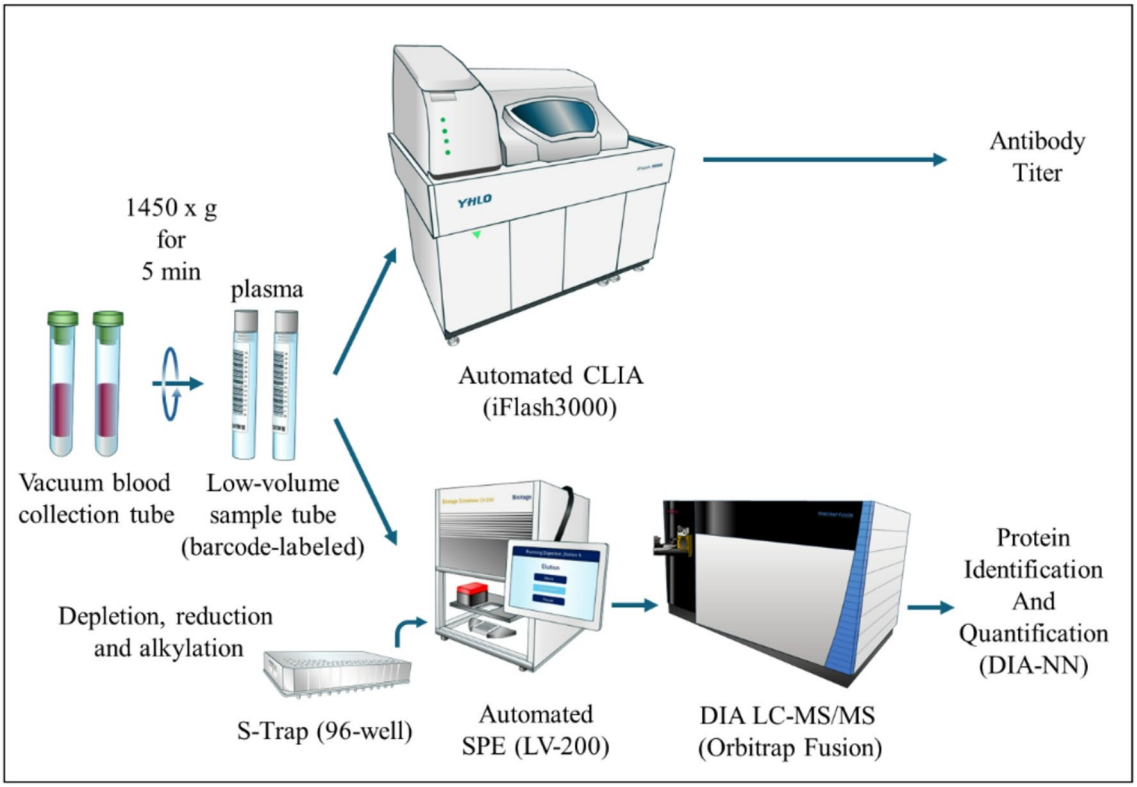

Fig. 1. Overview of the experimental workflow for plasma proteomics and antibody analysis. Peripheral blood samples were collected in vacuum blood collection tubes. Blood samples were centrifuged using a KUBOTA A3740 centrifuge (KUBOTA Corporation, Japan) with an SF-240 swinging-bucket rotor at 3000 rpm (1450 × g) for 5 min at room temperature. Plasma was then separated and aliquoted. Two parallel analyses were performed from the same plasma sample: (1) Antibody profiling: Plasma was subjected to automated chemiluminescent immunoassay (CLIA) using the iFlash 3000 (YHLO) to measure IgG antibody titers against SARS-CoV-2 antigens. (2) Proteome analysis: Proteins were extracted using the Extrahera LV-200 automated solid-phase extraction system (Biotage, Uppsala, Sweden), followed by sample preparation using the S-Trap (96-well) protocol. In this study, stringent SDS removal was performed during the S-Trap cleanup process using the Extrahera LV-200: SDS-containing samples were trapped in the S-Trap column and washed five times with 90% methanol/100 mM TEAB buffer (pH 7.1) to ensure complete SDS elimination. The resulting peptides were analyzed by data-independent acquisition (DIA) using Orbitrap Fusion LC-MS/MS (Thermo Fisher Scientific), and protein identification and quantification were performed using DIA-NN software.

Methods

Samples

An overview of the entire experimental workflow is shown in Fig. 1. The samples used in this study consisted of 18 human plasma samples collected from a single volunteer donor through blood sampling between August 18, 2021, and June 22, 2022. A 54-year-old male volunteer with well-controlled mild bronchial asthma participated in this study. He was on regular medication for asthma management but had no other chronic illnesses and maintained overall good health. He had received two doses of mRNA-based COVID-19 vaccination, with the last dose administered six months before infection onset. The management of these samples was conducted in accordance with institutional guidelines (The University of Tokyo) to ensure anonymity. The research involving these samples was approved by the Ethics Committee established at the University of Tokyo (Approval Number: 23–230).

Reagents

Protease inhibitor (Protease Inhibitor Cocktail Tablets, complete, Mini, EDTA-free Tablets) was purchased from Roche Diagnostics (Indianapolis, USA). Benzonase (Benzonase® endonuclease, purity grade I (≥99%) suitable for biopharmaceutical production) was obtained from Merck (Darmstadt, Germany). Phosphate-buffered saline (PBS), ammonium bicarbonate (AMBIC), dithiothreitol (DTT), iodoacetamide (IAA), and triethylammonium bicarbonate (TEAB) were acquired from Sigma (St. Louis, MO, USA). For the depletion of plasma samples, the Albumin and IgG Removal Kit (Amersham Biosciences, UK) was used. Sequencing-grade trypsin was purchased from Promega (Madison, WI, USA). BCA reagent was obtained from Thermo Fisher Scientific (Pierce Biotechnology, Madison, WI, USA). Acetonitrile, trifluoroacetic acid, formic acid, and methanol were procured from Kanto Chemical Co. Ltd. (Tokyo, Japan). SDS was purchased from Amersham Biosciences (Amersham,

UK). Phosphoric acid was obtained from Nacalai Tesque, Inc. (Kyoto, Japan). All water used in this study was produced via a Milli-Q system (Merck Millipore, Billerica, MA, USA).

For S-Trap processing, the following buffers and reaction solutions were prepared: 5% SDS in 50 mM TEAB (pH 7.55), 12% phosphoric acid, 90% methanol in 100 mM TEAB (pH 7.1), 50 mM TEAB (pH 8), 0.2% formic acid, and 0.2% formic acid in 50% ACN.

Antibody assay using iFlash 3000

In parallel with the proteomic analysis, plasma antibody titers against SARS-CoV-2 were measured. Blood samples were collected into vacuum blood collection tubes (for plasma separation), followed by centrifugation at 1,450 x g for 5 min at room temperature. The supernatant plasma was carefully recovered and subjected to a chemiluminescence immunoassay (CLIA).

Plasma antibody titers against SARS-CoV-2 were quantified using the fully automated chemiluminescent immunoassay (CLIA) analyzer iFlash 3000 (Shenzhen YHLO Biotech Co., Ltd., China). The assays included IgG antibodies targeting the nucleocapsid (N), spike subunit 1 (S1), and receptor-binding domain (RBD) antigens, as well as neutralizing antibodies (NAbs). All measurements were carried out with manufacturer-supplied reagent kits, applying a positivity threshold of 10 AU/mL.

The iFlash system employs paramagnetic microparticle-based CLIA technology, enabling high-throughput and multiplexed detection. The neutralization assay is based on a surrogate virus neutralization test (sVNT), which evaluates the inhibition of ACE2 binding to RBD-coated particles and thereby provides functional information on antibody-mediated neutralization. Calibration was performed using lot-specific QR code-encoded master curves with dedicated calibrators (CAL1 and CAL2 or CAL1-CAL4, depending on the assay), and internal quality controls at two concentration levels were included in each run according to the manufacturer's instructions (IFU, version 5.0, 2020). The reproducibility of the iFlash assays has been validated to ≤ 8% CV, with high sensitivity and specificity demonstrated in previous evaluations (Fig. 1)[9–13].

Sample preparation for DIA-LC-MS

For DIA-based LC-MS proteomics, plasma samples were processed according to the workflow shown in Fig. 1. Briefly, albumin and IgG were first depleted using the Albumin and IgG Removal Kit (Amersham Biosciences, UK). The depleted flow-through was then subjected to protein quantification and downstream preparation steps (precipitation, solubilization, reduction/alkylation, and S-Trap digestion) as described below.

First, the resin in the vial was thoroughly mixed to create a suspension, and an appropriate amount (approximately 5 mL) was transferred to a 15 mL tube. The resin was subsequently washed three times with PBS. A total of 15 µL of plasma was added to 750 µL of the resin slurry, and the mixture was mixed at room temperature (21 °C) for 30 min using a ThermoMixer (Eppendorf ThermoMixer comfort, Eppendorf, Hamburg, Germany) at 1400 rpm (mixing speed).

The mixture was then subjected to centrifugation using a spin column (6500 × g, 5 min), and the flowthrough was collected. The BCA protein assay was conducted to quantify the protein amount, and the results revealed a total protein quantity of 2.1–2.3 mg.

Next, TCA-acetone precipitation was performed, and the collected precipitate was dissolved in 5% SDS in 50 mM TEAB (pH 7.55), resulting in a total volume of 50 µL. Subsequently, reduction and alkylation of the sample were carried out. Then, 1 M DTT was added to achieve a final concentration of 20 mM, followed by incubation at 95 °C for 10 min and then a return to room temperature. Next, 1 M IAA was added to achieve a final concentration of 40 mM, and the sample was incubated in the dark at room temperature for 30 min. After reduction and alkylation, 12% phosphoric acid was added to the sample mixture to achieve a final concentration of 1.2%. A total of 350 µL of 90% methanol in 100 mM TEAB (pH 7.1) was added to bring the total volume to 405 µL. The sample was then subjected to S-Trap 96-well processing. The sample was gently transferred to S-Trap 96-well plate, to which 250 µL of 90% methanol in 100 mM TEAB (pH 7.1) was added for protein retention and subsequent washing of the retained proteins. This operation was repeated four times consecutively. Extrahera LV-200 (Biotage, Uppsala, Sweden) was used for these steps (Fig. 1).

Then, 250 µL of 50 mM TEAB was added to 20 µg/vial of trypsin (Promega) for dissolution, and 125 µL of this solution was immediately added to the S-Trap 96-well, which was then centrifuged at 4000 × g for 1 min. After incubation at 47 °C for 60 min, the reaction was continued overnight at 37 °C. The S-Trap 96-well plate was set on the Extrahera LV-200, and 80 µL of 50 mM TEAB was added to recover the flowthrough. Subsequently, 80 µL of 0.2% HCOOH was added, and the flowthrough was collected. Furthermore, 80 µL of 0.2% HCOOH in 50% ACN was added, followed by centrifugation at 4000 × g for 1 min to separate the flowthrough, which was then collected. After drying using a SpeedVac, the recovered samples were reconstituted in 200 µL of 0.1% TFA in 2% ACN.

LC-MS/MS conditions

The eluted samples were separated by nanoflow reverse-phase LC and analyzed on an Orbitrap Fusion mass spectrometer (Thermo Fisher Scientific, San Jose, CA, USA) equipped with a nano-electrospray ionization source[14-19]. The LC system was an Advance UHPLC (Bruker Daltonics, Bremen, Germany) with an HTS PAL autosampler (CTC Analytics, Zwingen, Switzerland). Peptides were separated on a reverse-phase column (L-column2 ODS, 3 µm, 0.2 × 150 mm; CERI, Tokyo, Japan) using mobile phase A (0.1% formic acid in water) and mobile phase B (0.1% formic acid in acetonitrile). The flow rate was 1.0 µL/min from 0 to 60 min and 1.2 µL/min thereafter. The LC gradient was as follows: 5% B at 0 min, ramped to 40% B over 60 min; increased to 95% B from 60 to 62 min; held at 95% B until 70 min; decreased to 5% B from 70 to 72 min; and held at 5% B until 80 min for re-equilibration. The total method duration was 79.9 min, consistent with the deposited raw acquisition method[20].

The mass spectrometer (Orbitrap Fusion, Thermo Fisher Scientific) was operated in data-independent acquisition (DIA) mode under Xcalibur control with a 3.0-s cycle time. MS1 spectra were acquired in the Orbitrap (60,000 resolution) over m/z 495–745 with an AGC target of 2.0×10^5 and a maximum injection time of 50 ms (profile, 1 microscan). DIA-MS2 spectra were acquired in the Orbitrap (30,000 resolution) using quadrupole isolation with staggered 4 m/z windows and 1 m/z overlap covering the precursor range m/z 498–742. The DIA isolation windows are summarized in the acquisition method, with an AGC target of 2.5×10^5 and a maximum injection time of 100 ms (centroid, 1 microscan). Fragmentation was performed by HCD at normalized collision energy (NCE) 30. The nano-electrospray ion source was operated at 1.7 kV (positive mode), with an ion transfer tube temperature of 280 °C, and internal lock-mass calibration was enabled (m/z 391.28429)[7,8,21].

DIA data processing

Raw data were processed using Data-Independent Acquisition by Neural Networks (DIA-NN) for proteome analysis. DIA-NN is known to be particularly useful for applications in high-throughput proteomics because it improves the performance of protein identification and quantification in conventional DIA-mode proteomics applications, enabling fast and reliable protein identification[6,22].

The algorithm for DIA-NN was as follows. DIA-NN version 1.8.1, in library-free mode, was used with the same UniProt FASTA database. The protein database was the UniProt Reference Proteome for Homo sapiens (Taxonomy 9606; Proteome ID UP000005640; 20,373 entries; UniProt release 2022_03; reviewed human canonical).

Precursors of charge states 1–4, peptide lengths 7–30, and peptide m/z 300–1800 were considered, with a maximum of one missed cleavage. A maximum of one variable modification per peptide was considered. Cysteine carbamidomethylation was allowed as a fixed modification, N-terminal methionine excision as a variable modification, methionine oxidation as a variable modification, and N-terminal acetylation as a variable modification. The precursor false discovery rate was then filtered at 1% FDR[6–8,21,22].

The raw and processed mass spectrometry data have been deposited in JPOST (JPST003696) and registered with ProteomeXchange (PXD062242).

Multivariate and differential expression analysis

Temporal proteomic dynamics were analyzed using Scaffold DIA (version 3.4.1, Proteome Software, Portland, OR, USA). DIA-MS results were imported into Scaffold DIA, and protein identifications were grouped by parsimony and filtered to a protein-level FDR of < 1.0%.

For differential abundance, the predefined pre-infection (Group A) and post-infection (Group B) phases were compared across all quantified proteins using an ANOVA-equivalent two-group comparison on log2-scaled intensities with Benjamini-Hochberg multiple-testing correction (BH-FDR). Differential results (p-values, BH-FDR, and log2FC [B-A]) are provided in Supplementary Tables 1, and volcano plots were generated to visualize effect sizes and statistical significance.

Proteins with a fold change ≥ 1.9 were additionally reported as an effect-size-based, hypothesis-generating "Top32" shortlist for visualization and exploratory discussion; these proteins are annotated with the same A/B statistics in Supplementary Table 2.

For heatmap visualization (Fig. 4), the Top 150 proteins with the largest absolute change (|Δ|) between Groups A and B were selected to enable stable clustering and maintain interpretability, and hierarchical clustering was used to define four clusters (k = 4). For pathway-level interpretation, functional enrichment analysis was performed using Enrichr with gene symbols as input[23–25] on the BH-FDR-defined significant protein set (BH-FDR < 0.05), and enrichment results (GO Biological Process / KEGG / Reactome; Top 20 terms) are summarized in Supplementary Table 3.

Results

Antibody titer dynamics following vaccination and infection

The results of antibody titers measured using the iFlash 3000 are summarized in Table 1; Fig. 2. As shown in the graph, both the S1 antigen and neutralizing antibody values increased markedly after the second vaccination. In contrast, the IgG antibody against the N antigen did not increase in response to vaccination. However, a sharp rise in the IgG N antigen antibody value was clearly observed following SARS-CoV-2 infection. Based on these findings, we proceeded to examine the proteomic profiles of the plasma samples using DIA-based analysis to identify proteins that showed a clear response associated with these antibody dynamics.

Building on the distinct antibody titer dynamics observed before and after vaccination and infection, we conducted a comprehensive plasma proteome analysis using data-independent acquisition (DIA)-based LC-MS/MS. This approach aimed to capture both qualitative and quantitative changes in plasma proteins corresponding to individual immune responses. Following protein identification and quantification, multivariate statistical analyses including principal component analysis (PCA) and heatmap clustering were performed to visualize longitudinal trends and identify characteristic protein expression patterns linked to these immunological events. To visualize coordinated temporal regulation, we focused on the Top 150 most dynamically changing proteins, which provided stable clustering structure and enabled robust cluster-level enrichment, while maintaining readability. These data provided a broader molecular context that complemented the antibody titer profiles and enabled the identification of potential biomarkers reflecting the host's systemic response to SARS-CoV-2 exposure.

Detailed information on plasma samples applied for DIA-proteome analysis								
Sample No.	Year	Date	After 1st vaccination, days	After 2nd vaccination, days	After infection, days	IgG S1 antigen antibody, AU/mL	Neutralizing activity, AU/mL	IgG N antigen antibody, AU/mL
1	2021	18-Aug	2	-	-	0.16	7.44	-
2		25-Aug	9	-	-	1.51	92	-
3		1-Sep	16	-	-	319	137	-
4		15-Sep	30	2	-	510	164	-
5		6-Oct	51	23	-	2682	1762	-
6		20-Oct	65	37	-	2283	1342	0.64
7		10-Nov	86	58	-	1806	1185	0.52
8		1-Dec	107	79	-	1186	720	0.43
9		22-Dec	128	100	-	1064	663	0.39
10	2022	12-Jan	149	121	-	834	618	0.43
11		2-Feb	170	142	-	721	376	0.51
12		2-Mar	198	170	-	448	269	0.49
13		16-Mar	212	184	-	478	228	0.49
14		30-Mar	226	198	13	2623	844	35.68
15		20-Apr	247	219	34	3822	923	37
16		11-May	268	240	55	3716	926	25
17		1-Jun	289	261	76	3099	927	22
18		22-Jun	310	282	97	3131	850	18

Table 1. Summary of antibody titers, collection dates, and DIA-based proteome analysis of human plasma samples. 1st Vaccination: August 16, 2021 (Moderna), 2nd Vaccination: September 13, 2021 (Moderna), SARS-CoV-2 infection: March 17, 2022 (PCR positive), March 23, 2022 (PCR negative).

Comprehensive multivariate analysis of plasma proteomes before and after SARS-CoV-2 infection

A total of 1,502 human proteins were identified from 18 longitudinal plasma samples using DIA-based LC-MS/MS. To understand the overall protein expression dynamics in relation to vaccination and infection events, multivariate statistical analyses were performed on the quantified proteomic data.

Principal component analysis (PCA) revealed a clear temporal shift in the global proteome profile, particularly distinguishing post-infection samples from pre-vaccination and post-vaccination ones (Fig. 3). The score plot showed that samples clustered along a trajectory corresponding to the volunteer's clinical course, with samples collected after infection forming a distinct group. This trend was further supported by hierarchical clustering of the top 150 most variable proteins, which grouped post-infection samples separately from earlier time points (Fig. 4).

These findings suggest that SARS-CoV-2 infection induces marked proteomic remodeling in the plasma, beyond the changes observed following vaccination. Based on these multivariate analyses, we next aimed to identify individual proteins that showed the most prominent upregulation after infection, using fold-change-based filtering.

Identification of the Top 32 most upregulated plasma proteins following SARS-CoV-2 infection

To further visualize the longitudinal changes in plasma proteins, a heatmap analysis was performed for all proteins identified by DIA-NN. To visualize coordinated temporal regulation, we focused on the Top 150 most dynamically changing proteins, which provided stable clustering structure and enabled robust cluster-level enrichment, while maintaining readability (Fig. 4).

To further identify key molecular events associated with SARS-CoV-2 infection, we extracted the top 32 plasma proteins that exhibited the highest upregulation based on fold change ($FC \geq 1.9$) in samples collected after infection. This subset was selected by comparing proteomic profiles before infection (samples 1–13) with those after infection (samples 14–18), as determined by DIA-based quantification.

The selected proteins are listed in Table 2, and their expression dynamics are visualized in Fig. 5 as a line graph. This graph highlights temporal increases in expression corresponding to the infection period. Several immune-related and inflammation-associated proteins were included in the top-ranked group, suggesting a strong host response to viral invasion. Notably, proteins such as CNOT1, RPL11, and GSDMA showed consistent upregulation after infection and aligned well with changes in N antigen antibody titers.

These results reinforce the potential utility of DIA-MS in capturing biologically relevant proteomic shifts during immune responses and provide candidate markers for future investigation into infection-induced pathways.

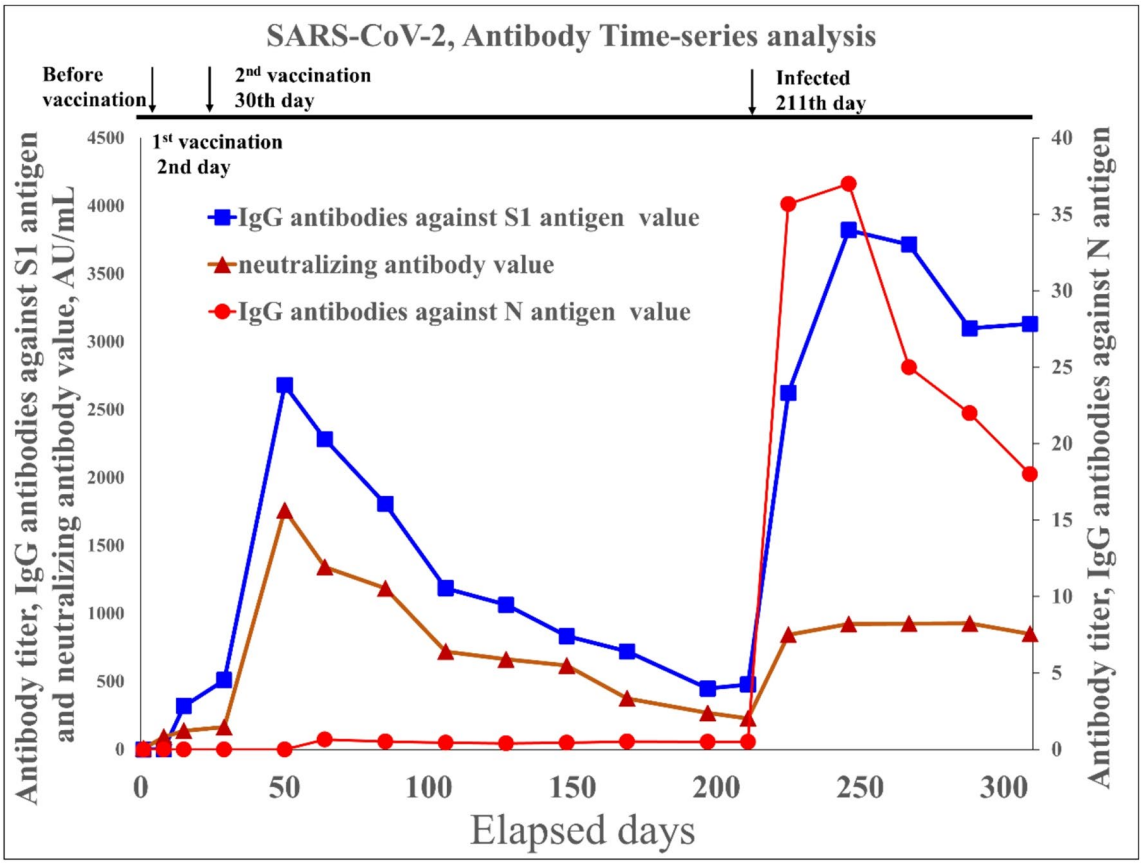

Fig. 2. Fluctuations in the antibody titers against SARS-CoV-2 in human plasma samples. Antibody titers in human plasma samples from a single donor were measured over a period of 310 days, from August 18, 2021, to June 22, 2022. The donor received their first dose of the vaccine (Moderna) two days after the initial blood collection, followed by the second dose 30 days later (Moderna). At 211 days after the sample collection date, the donor became infected with SARS-CoV-2.

Differential expression analysis to identify significantly regulated proteins

To visualize global changes in plasma protein abundance associated with vaccination and subsequent SARS-CoV-2 infection, volcano plots were generated and overlaid across three longitudinal comparisons using Scaffold DIA-derived quantitative data. The plots illustrate the overall distribution of fold changes and statistical significance, highlighting a subset of proteins showing marked abundance changes following infection.

To visualize proteins showing marked changes after SARS-CoV-2 infection, we generated a volcano plot based on the DIA-MS quantitative data (Fig. 6). The analysis compared samples collected before infection (samples 1–13) and after infection (samples 14–18), using fold change and unadjusted p-value thresholds as displayed in Scaffold DIA; BH-FDR-controlled statistics are provided separately in Supplementary Table 1.

As shown in Table 2; Fig. 5, multiple proteins were identified as significantly upregulated in the post-infection group. Proteins such as CNOT1, RPL11, and GSDMA showed both high statistical significance and large fold changes, highlighting them as candidate infection-associated proteins in this individual of infection-associated immune responses. Conversely, proteins such as U1SBP (Q16560) were downregulated and may reflect suppressed pathways or altered transcriptional activity following infection (Supplementary Fig. 1).

The volcano plot visualization provided a clear and intuitive representation of the global proteomic changes induced by SARS-CoV-2 infection and allowed for the prioritization of proteins for downstream validation and mechanistic exploration.

Proteomic characterization based on the top 32 most upregulated proteins

To explore proteomic trends associated with the host response to SARS-CoV-2 infection, we extracted the top 32 most upregulated plasma proteins based on fold change values comparing post-infection samples (No. 14–18) to pre-infection samples (No. 1–13). The selected proteins exhibited fold changes ≥ 1.9 and encompassed a broad range of functional categories (Table 2).

Notably, these proteins included molecules associated with transcription/translation (e.g., CNOT1, RPL11), cytoskeletal regulation (e.g., KRT19, KRT17, NEB), immune responses (e.g., ANXA1, S100P, NOTCH4, IGHV4-4), and protein degradation (e.g., PSMA7). The diversity of protein classes suggests a systemic biological response, including inflammation, immune activation, structural remodeling, and potential epigenetic regulation.

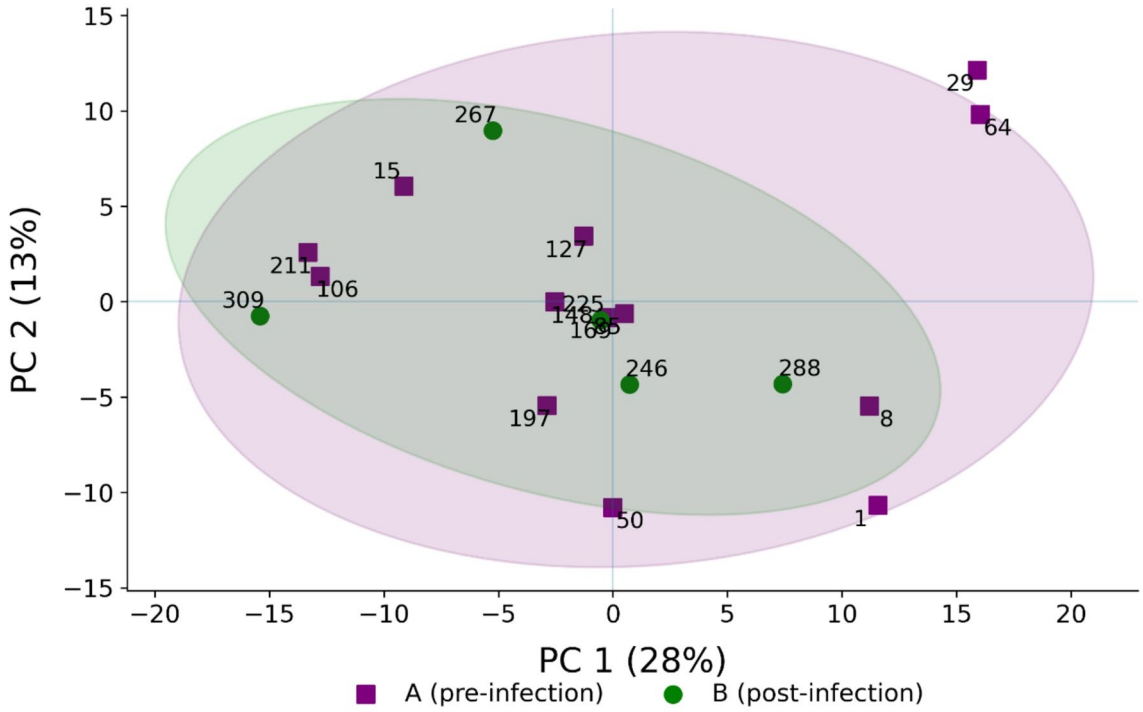

Fig. 3. Scores plot of Principal Component Analysis (PCA) using quantified protein expression data from plasma samples. Each point represents an individual sample, with purple squares (▪) indicating pre-infection samples (Group A) and green circles (●) representing post-infection samples (Group B). The first two principal components, PC1 (28%) and PC2 (13%), explain 41% of the total variance. While the two groups partially overlap, a moderate shift in the distribution of Group B toward the negative side of PC1 suggests systematic proteomic changes associated with SARS-CoV-2 infection.

Among these, the 60 S ribosomal protein L11 (RPL11) and CCR4-NOT complex subunit 1 (CNOT1) showed particularly high fold changes (> 7.0 and 40.0, respectively), indicating marked upregulation of the translational machinery. Also of note were S100P and Gasdermin-A, implicating inflammatory and pyroptotic responses.

These observations suggest that SARS-CoV-2 infection induces broad molecular alterations beyond conventional immunoglobulin responses, potentially involving post-transcriptional and cytoskeletal remodeling processes. Further mechanistic validation is warranted, and detailed interpretation of these changes is discussed in the following section (Discussion).

Discussion

In this study, we demonstrated that the parallel application of SARS-CoV-2 antibody testing and DIA-based LC-MS/MS proteome profiling to the same plasma samples enabled time-resolved visualization of protein dynamics associated with antibody titer fluctuations. This integrative approach led to the identification of candidate biomarkers and provided insight into host responses to SARS-CoV-2 infection.

Comprehensive multivariate analysis—including PCA, heatmaps, and volcano plots—highlighted distinct post-infection expression patterns. In particular, the upregulation of 60 S ribosomal protein L11 (RPL11) was observed following SARS-CoV-2 infection in this individual. RPL11 is a structural component of the large ribosomal subunit and is also involved in p53-mediated stress responses and ribosomal biogenesis regulation[26–31]. In the context of this single-subject longitudinal analysis, the observed increase in RPL11 is presented as an illustrative example of infection-associated proteomic dynamics rather than evidence of a generalized host response. These findings are consistent with previous reports describing alterations in ribosomal proteins during SARS-CoV-2 infection[23–25], while requiring validation in independent cohorts.

Notably, CNOT1 exhibited the highest fold change (> 40-fold) among all proteins identified in this screening analysis. As a scaffold DIA protein of the CCR4-NOT complex, CNOT1 is known to regulate mRNA deadenylation, transcriptional repression, and immune-related signaling pathways. In the context of this single-subject longitudinal study, its marked induction may reflect infection-associated activation of post-transcriptional regulatory processes, rather than serving as evidence for a generalized host response.

In addition to translational machinery components, we also observed elevated expression of immune modulators (e.g., ANXA1, S100P, NOTCH4), cytoskeletal proteins (e.g., KRT17, KRT19), and inflammation-related factors (e.g., GSDMA). These changes suggest a broad host response involving inflammation, immune regulation, and tissue remodeling.

Conversely, some nuclear regulatory proteins such as U1SBP (Q16560) were markedly downregulated. This protein is associated with pre-mRNA splicing and transcription regulation, and its loss may imply compromised

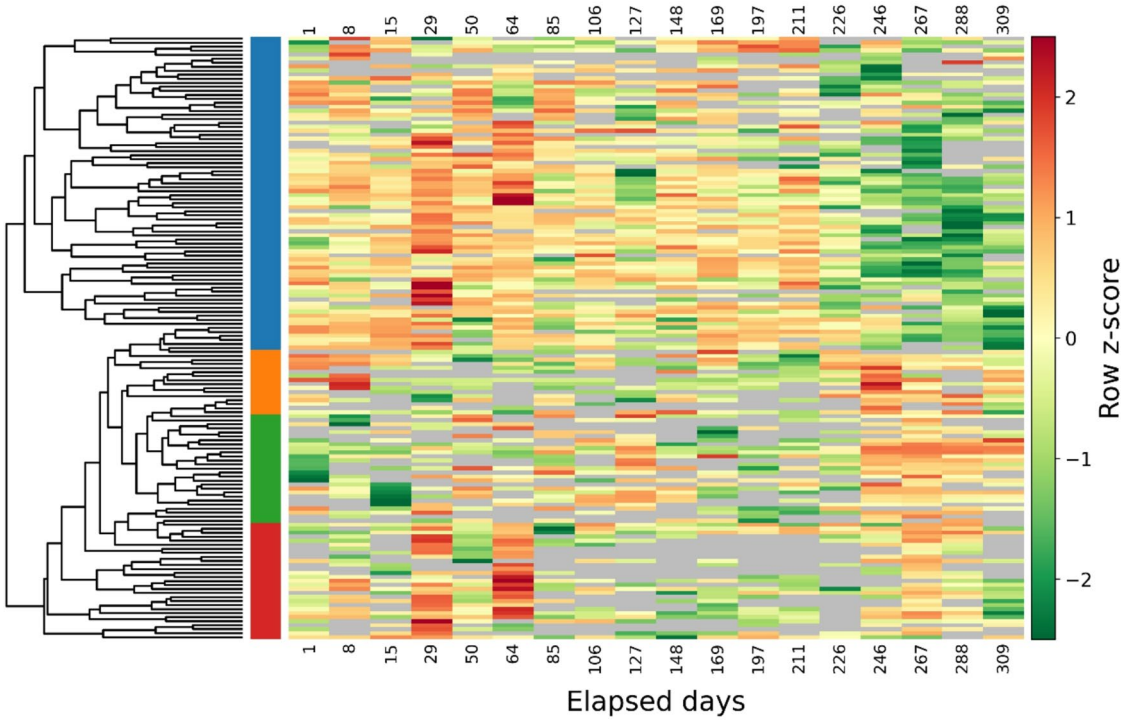

Fig. 4. Heatmap depicting the quantitative expression profiles of all proteins identified in longitudinal plasma samples using DIA-based proteome analysis. The heatmap displays the Top 150 most dynamically regulated proteins (ranked by the largest absolute pre- vs. post-infection change). This number was chosen to obtain stable clustering and enrichment while maintaining figure readability. The Top 150 set is used for visualization; statistical inference is based on the FDR-defined significant protein set.

nuclear RNA processing. Such dysregulation could impair stress recovery or exacerbate disease progression, especially in immunocompromised individuals[31–34]. While beyond the scope of the present study, this observation will be prioritized in future validation studies.

Overall, this study highlights the utility of integrated antibody profiling and DIA-based plasma proteomics for time-resolved, within-subject characterization of SARS-CoV-2-associated proteomic dynamics. The observed changes, including RPL11 and CNOT1, are presented as hypothesis-generating signals that warrant validation in independent cohorts and follow-up studies. Several large-scale studies have already profiled longitudinal plasma proteomic changes associated with SARS-CoV-2 infection and vaccination[35–42]. In contrast, the present work is a single-case, within-subject longitudinal follow-up with matched serology, intended as a hypothesis-generating illustration of temporal proteomic dynamics rather than population-level validation.

These findings suggest that combined proteome and antibody analyses may provide novel insights into host responses against SARS-CoV-2 infection and support the development of new biomarkers and therapeutic targets. However, this study has certain limitations. In addition, the study participant had well-controlled asthma under regular treatment, and while IL-6 was not reliably quantified by the DIA-based proteomics workflow and CRP did not show significant temporal variation, we cannot exclude that underlying inflammatory conditions or their treatment may influence baseline proteomic profiles in a single-subject study. Neutralizing antibody assays, such as pseudovirus-based tests, were not performed, which may restrict the interpretation of functional immune responses. Addressing this point will be an important task in future investigations.

Protein (name)	Accession Number	Gene Name	Category	Family	Fold Change
CCR4-NOT transcription complex subunit 1	A5YKK6	CNOT1	-	Other	40.0
Gasdermin-A	Q96QA5	GSDMA	Infection/ Stress	Gasdermin family	8.2
RB1-inducible coiled-coil protein 1	Q8TDY2	RB1CC1	-	Other	8.1
Large ribosomal subunit protein uL5	P62913	RPL11	Transcription/ Translation	Ribosomal protein	7.3
Dynein axonemal assembly factor 1	Q8NEP3	DNAAF1	Transcription/ Translation	Dynein-related	6.2
Keratin, type I cytoskeletal 19	P08727	KRT19	Cytoskeleton	Keratin family	5.1
Nebulin	P20929	NEB	-	Other	4.4
C3 and PZP-like alpha-2-macroglobulin domain-containing protein 8	Q8IZJ3	CPAMD8	-	Other	3.5
Annexin A1	P04083	ANXA1	Immunity	Annexin family	3.3
Keratin, type I cuticular Ha1	Q15323	KRT31	Cytoskeleton	Keratin family	2.8
Neurogenic locus notch homolog protein 4	Q99466	NOTCH4	Immunity	Notch family	2.6
Protein S100-P	P25815	S100P	Immunity	S100 family	2.6
Trafficking protein particle complex subunit 12	Q8WVT3	TRAPPC12	-	Other	2.6
Serine protease inhibitor Kazal-type 5	Q9NQ38	SPINK5	-	Other	2.5
WAS/WASL-interacting protein family member 3	A6NGB9	WIPF3	-	Other	2.5
Keratin, type II cuticular Hb2	Q9NSB4	KRT82	-	Keratin family	2.5
Keratin, type I cytoskeletal 17	Q04695	KRT17	Cytoskeleton	Keratin family	2.5
Endosialin	Q9HCU0	CD248	Immunity	Other	2.4
RNA cytidine acetyltransferase	Q9H0A0	NAT10	Transcription/ Translation	Other	2.2
Keratin, type II cytoskeletal 6 A	P02538	KRT6A	-	Keratin family	2.1
Protein S100-A7	P31151	S100A7	Immunity	S100 family	2.1
Immunoglobulin heavy variable 4–4	A0A075B6R2	IGHV4-4	-	Immunoglobulin family	2.1
Proteasome subunit alpha type-7	O14818	PSMA7	Protein degradation	Proteasome family	2.0
Leucine-rich repeat-containing protein 15	Q8TF66	LRRC15	-	Other	2.0
Immunoglobulin heavy variable 1–45	A0A0A0MS14	IGHV1-45	-	Immunoglobulin family	2.0
Keratin, type I cuticular Ha3-II	Q14525	KRT33B	-	Keratin family	2.0
Vinculin	P18206	VCL	Cytoskeleton	Other	2.0
Rho guanine nucleotide exchange factor 2	Q92974	ARHGEF2	Transcription/ Translation	Other	1.9
Synaptophysin-like protein 1	Q16563	SYPL1	-	Other	1.9
Immunoglobulin kappa variable 2D-28	P01615	IGKV2D-28	-	Immunoglobulin family	1.9
Immunoglobulin lambda variable 3–12	A0A075B6K2	IGLV3-12	Immunity	Immunoglobulin family	1.9
Hepatocyte growth factor receptor	P08581	MET	Receptor	MET receptor family	1.9

Table 2. Top 32 plasma proteins showing increased abundance following SARS-CoV-2 infection. This table lists the top 32 plasma proteins that showed increased abundance after SARS-CoV-2 infection, as identified by DIA-NN analysis. Proteins were selected based on a fold change (post-infection vs. pre-infection) ≥ 1.9. For each protein, the function or interpretation, UniProt accession number, gene name, functional category, protein family, and fold change are provided. Categories include immunity-related proteins, cytoskeletal components, and transcription/translation-associated proteins, among others. This classification aids in understanding the biological relevance of the proteomic changes observed in the longitudinal study. Fold change (FC) was calculated as the median of post-infection samples (No. 14–18) divided by the median of pre-infection samples (No. 1–13). Accession Number follows UniProt; Gene Name follows HGNC. Category/ Family indicates concise functional grouping. FC: fold change.

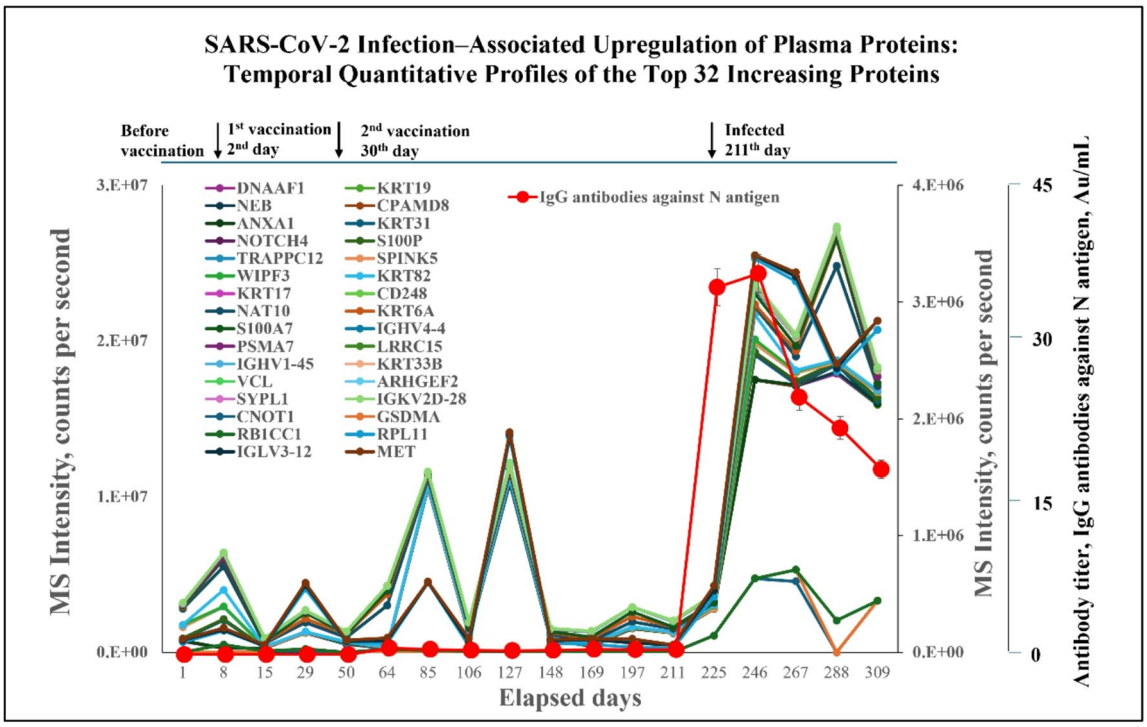

Fig. 5. Temporal expression profiles of the top 32 upregulated plasma proteins following SARS-CoV-2 infection. Proteins were selected from all quantified proteins based on a fold change ≥ 1.9, as determined by DIA-NN analysis. The line graph shows the MS intensity (counts per second) of each protein across 18 time points over a 310-day period. The red line indicates IgG antibody titers against the SARS-CoV-2 N antigen, measured using the iFlash 3000 (right axis). A sharp increase in both IgG levels and MS intensities of selected proteins was observed after SARS-CoV-2 infection on day 211, whereas minimal changes were seen before and after vaccination.

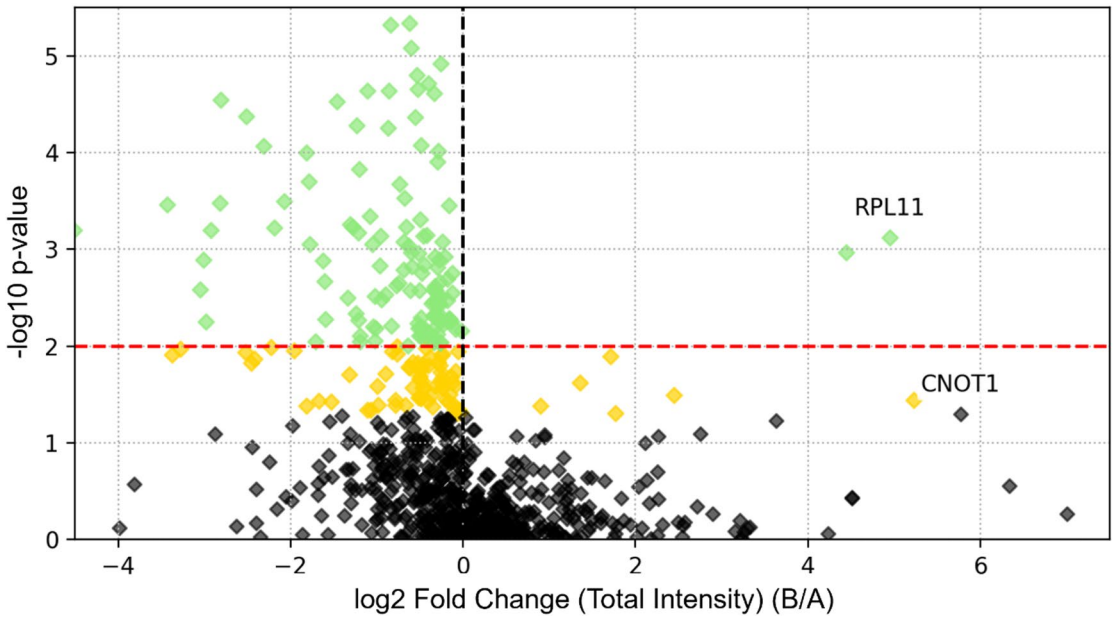

Fig. 6. Overlayed volcano plot summarizing differential plasma protein abundance across longitudinal comparisons. Volcano plots generated in Scaffold DIA were re-plotted using the extracted numerical values, and the three comparisons (comp1-comp3) were overlaid in a single panel. The x-axis shows log2 fold change (Total Intensity; B/A), and the y-axis shows −log10 p-value. Points are colored according to significance categories used by Scaffold DIA: green ("Significant") indicates proteins with $p < 0.01$ ($-\log10\ p \geq 2.0$); yellow ("Sig. w/o correction") indicates proteins with $0.01 \leq p < 0.05$ ($1.301 \leq -\log10\ p < 2.0$) without multiple-testing correction; black ("Not significant") indicates proteins with $p \geq 0.05$ ($-\log10\ p < 1.301$). The red dashed horizontal line marks $p = 0.01$, and the vertical dashed line marks log2 fold change = 0. Gene symbols are shown only for representative proteins discussed in the text (CNOT1 and RPL11); full protein identifiers and Group A vs. Group B differential abundance statistics (p-values, BH-FDR, and log2FC [B-A]) are provided in Supplementary Table 1.

Data availability

The raw and processed mass spectrometry data have been deposited in JPOST (JPST003696) and registered with ProteomeXchange (PXD062242).

Received: 22 August 2025; Accepted: 9 April 2026
Published online: 19 April 2026

References

1. Shuai, H. et al. Attenuated replication and pathogenicity of SARS-CoV-2 B.1.1.529 Omicron. *Nature* **603**, 693–699 (2022).
2. Suzuki, R. et al. Attenuated fusogenicity and pathogenicity of SARS-CoV-2 Omicron variant. *Nature* **603**, 700–705 (2022).
3. Marcelin, J. R. et al. COVID-19 Vaccines and SARS-CoV-2 Transmission in the Era of New Variants: A Review and Perspective. *Open. Forum Infect. Dis.* **9**, ofac124 (2022).
4. Silva, S. J. R., Kohl, A., Pena, L. & Pardee, K. Recent insights into SARS-CoV-2 omicron variant. *Rev. Med. Virol.* **33**, e2373 (2023).
5. Zhang, F., Ge, W., Ruan, G., Cai, X. & Guo, T. Data-Independent Acquisition Mass Spectrometry-Based Proteomics and Software Tools: A Glimpse in 2020. *Proteomics* **20**, e1900276 (2020).
6. Demichev, V., Messner, C. B., Vernardis, S. I., Lilley, K. S. & Ralser, M. DIA-NN: neural networks and interference correction enable deep proteome coverage in high throughput. *Nat. Methods*. **17**, 41–44 (2020).
7. Jiang, N. et al. A data-independent acquisition (DIA)-based quantification workflow for proteome analysis of 5000 cells. *J. Pharm. Biomed. Anal.* **216**, 114795 (2022).
8. Gotti, C. et al. DIA proteomics data from a UPS1-spiked. *Data Brief.* **41**, 107829 (2022).
9. Kaneko, Y. et al. The serological diversity of serum IgG/IgA/IgM against SARS-CoV-2 nucleoprotein, spike, and receptor-binding domain and neutralizing antibodies in patients with COVID-19 in Japan. *Health Sci. Rep.* **5**, e572. https://doi.org/10.1002/hsr2.572 (2022).
10. Yokoyama, T. et al. Comprehensive proteome analysis of longitudinal plasma samples from a single donor after SARS-CoV-2 infection. *PLoS One*. **16**, e0247711. https://doi.org/10.1371/journal.pone.0247711 (2021).
11. Nakamura, N., Kobashi, Y. & Kim, K. S. Modeling and predicting individual variation in COVID-19 vaccine-elicited antibody response in the general population. *PLoS Digit. Health*. **3**, e0000497. https://doi.org/10.1371/journal.pdig.0000497 (2024).
12. Yoshida, M., Kobashi, Y. & Kawamura, T. Factors associated with COVID-19 vaccine booster hesitancy: a retrospective cohort study. *Fukushima Vaccination Community Surv. Vaccines*. **10**, 515. https://doi.org/10.3390/vaccines10040515 (2022).
13. Saito, H., Yoshimura, H. & Yoshida, M. Antibody profiling of microbial antigens in the blood of COVID-19 mRNA vaccine recipients using microbial protein microarrays. *Vaccines* **11**, 1694 (2023).
14. Obi, N. et al. Development of drug discovery screening system by molecular interaction kinetics-mass spectrometry. *Rapid Commun. Mass. Spectrom.* **32**, 665–671 (2018).
15. Fukuda, T. et al. An improvement on mass spectrometry-based epigenetic analysis of large histone-derived peptides by using the Ionization Variable Unit interface. *Anal. Biochem.* **486**, 14–16 (2015).

16. Kawamura, T. et al. Proteomic analysis of laser-microdissected paraffin-embedded tissues: (1) Stage-related protein candidates upon non-metastatic lung adenocarcinoma. *J. Proteom.* **73**, 1089–1099 (2010).
17. Nishimura, T. et al. Proteomic analysis of laser-microdissected paraffin-embedded tissues: (2) MRM assay for stage-related proteins upon non-metastatic lung adenocarcinoma. *J. Proteom.* **73**, 1100–1110 (2010).
18. Fukuda, T. et al. A selected reaction monitoring mass spectrometric assessment of biomarker candidates diagnosing large-cell neuroendocrine lung carcinoma by the scaling method using endogenous references. *PLoS One*. **12**, e0176219 (2017).
19. Wang, J., Luzum, J. A., Phelps, M. A. & Kitzmiller, J. P. Liquid chromatography-tandem mass spectrometry assay for the simultaneous quantification of simvastatin, lovastatin, atorvastatin, and their major metabolites in human plasma. *J. Chromatogr. B Analyt Technol. Biomed. Life Sci.* **983–984**, 18–25 (2015).
20. Kosuge, H. et al. Proteomic identification and validation of novel interactions of the putative tumor suppressor PRELP with membrane proteins including IGFI-R and p75NTR. *J. Biol. Chem.* **296**, 100278 (2021).
21. Mosquim Junior, S., Siino, V., Rydén, L., Vallon-Christersson, J. & Levander, F. Choice of high-throughput proteomics method affects data integration with transcriptomics and the potential use in biomarker discovery. *Cancers* **14**, 5761 (2022).
22. Demichev, V. et al. dia-PASEF data analysis using FragPipe and DIA-NN for deep proteomics of low sample amounts. *Nat. Commun.* **13**, 3944 (2022).
23. Kuleshov, M. V. et al. Enrichr: a comprehensive gene set enrichment analysis web server 2016 update. *Nucleic Acids Res.* **44** (W1), W90–W97 (2016).
24. Gene Ontology Consortium. The Gene Ontology resource: enriching a GOld mine. *Nucleic Acids Res.* **49**, D325–D334 (2021).
25. Kanehisa, M. & Goto, S. KEGG: kyoto encyclopedia of genes and genomes. *Nucleic Acids Res.* **28**, 27–30 (2000).
26. Gray, J. P. et al. The ribosomal protein rpL11 associates with and inhibits the transcriptional activity of peroxisome proliferator-activated receptor-alpha. *Toxicol. Sci.* **89**, 535–546 (2006).
27. Zhu, Q. et al. Up-regulated 60S ribosomal protein L18 in PEDV N protein-induced S-phase arrested host cells promotes viral replication. *Virus Res.* **321**, 198916 (2022).
28. Khalid, Z. et al. Identification of novel therapeutic candidates against SARS-CoV-2 infections: An application of RNA sequencing toward mRNA-based nanotherapeutics. *Front. Microbiol.* **13**, 901848 (2022).
29. Luan, Y. et al. Deficiency of ribosomal proteins reshapes the transcriptional and translational landscape in human cells. *Nucleic Acids Res.* **50**, 6601–6617 (2022).
30. Chakraborty, A. et al. Cross talk between TP53 and c-Myc in the pathophysiology of Diamond-Blackfan anemia: Evidence from RPL11-deficient in vivo and in vitro models. *Biochem. Biophys. Res. Commun.* **495**, 1839–1845 (2018).
31. Devlin, J. R. et al. Combination therapy targeting ribosome biogenesis and mRNA translation synergistically extends survival in MYC-driven lymphoma. *Cancer Discov.* **6**, 59–70 (2016).
32. Cao, P. et al. Genomic gain of RRS1 promotes hepatocellular carcinoma through reducing the RPL11-MDM2-p53 signaling. *Sci. Adv.* **7** (35), eabf4304. https://doi.org/10.1126/sciadv.abf4304 (2021).
33. Li, H. et al. Loss of RPS27a expression regulates the cell cycle, apoptosis, and proliferation via the RPL11-MDM2-p53 pathway in lung adenocarcinoma cells. *J. Exp. Clin. Cancer Res.* **41**, 33 (2022).
34. Will, C. L., Schneider, C., Reed, R. & Luhrmann, R. Identification of both shared and distinct proteins in the major and minor spliceosomes. *Science* **284**, 2003–2005 (1999).
35. Will, C. L. et al. The human 18S U11/U12 snRNP contains a set of novel proteins not found in the U2-dependent spliceosome. *RNA* **10**, 929–941 (2004).
36. Niemela, E. H., Verbeeren, J., Singha, P., Nurmi, V. & Frilander, M. J. Evolutionarily conserved exon definition interactions with U11 snRNP mediate alternative splicing regulation on U11-48K and U11/U12-65K genes. *RNA Biol.* **12**, 1256–1264 (2015).
37. Hall, S. L. & Padgett, R. A. Requirement of U12 snRNA for in vivo splicing of a minor class of eukaryotic nuclear pre-mRNA introns. *Science* **271**, 1716–1718 (1996).
38. Shen, B. et al. Proteomic and metabolomic characterization of COVID-19 patient sera. *Cell* **182**, 59–72e15 (2020).
39. Messner, C. B. et al. Ultra-high-throughput clinical proteomics reveals classifiers of SARS-CoV-2 infection. *Cell. Syst.* **11**, 11–24e4 (2020).
40. Del Valle, D. M. et al. An inflammatory cytokine signature predicts COVID-19 severity and survival. *Nat. Med.* **26**, 1636–1643 (2020).
41. Viode, A. et al. Longitudinal plasma proteomic analysis of 1117 hospitalized patients with COVID-19 identifies features associated with severity and outcomes. *Sci. Adv.* **10**, eadl5762 (2024).
42. Wang, Y. et al. Longitudinal proteomic profiling of COVID-19 vaccination. *Protein Cell.* **14**, 668–682 (2023).

Acknowledgements

We would like to express our sincere appreciation to Ms. Akiko Fukuda (Laboratory for Systems Biology and Medicine, Isotope Science Center, The University of Tokyo) for her invaluable assistance in conducting the antibody titer measurements, and to Ms. Noriko Kagi (Biotage Japan Ltd., Tokyo, Japan) for her expert technical support with the LV-200 experiments.

Author contributions

Author ContributionsT.F. performed plasma sample preprocessing, DIA-LC–MS analysis, data evaluation, and verification of analytical accuracy and validity. He also prepared all tables and figures and wrote the main text of the manuscript.A.N. conducted antibody titer measurements and performed DIA-LC–MS sample measurements.Y.C. examined the DIA-LC–MS results and analyzed the data using DIA-NN.Y.B. supervised the experimental application of DIA-NN and the S-Trap method.T.K. verified the accuracy and validity of antibody assays and DIA-LC–MS analysis, and supervised the overall progress of the study.All authors reviewed and approved the final manuscript.

Funding

This study was supported by Medical & Biological Laboratories Co., Ltd., and Shenzhen YHLO Biotech Co., Ltd. (the distributor and manufacturer of the antibody measurement system, iFlash 3000); by grants from Peace Winds Japan, Kowa Co., and the Research Center for Advanced Science and Technology at the University of Tokyo; and by the Japan Agency for Medical Research and Development (AMED) under the Grant-in-Aid for the Development of Vaccines for the Novel Coronavirus Disease (Grant Number: 22nf0101638h0002).

Declarations

Declaration of generative AI and AI-assisted technologies in the writing process

During the preparation of this work, the author used ChatGPT (OpenAI) to improve the clarity and readability of the manuscript. After using this tool, the authors reviewed and edited the content as needed and took full responsibility for the content of the publication.

Competing interests

The authors declare no competing interests.

Ethical approval and consent to participate

This study was approved by the Institutional Ethics Committee of The University of Tokyo (approval number: 23–230). Informed consent was obtained from all individual participants included in the study.

Additional information

Supplementary Information The online version contains supplementary material available at https://doi.org/10.1038/s41598-026-48765-z.

Correspondence and requests for materials should be addressed to T.F. or T.K.

Reprints and permissions information is available at www.nature.com/reprints.

Publisher's Note Springer Nature remains neutral with regard to jurisdictional claims in published maps and institutional affiliations.